

553 **1 Introduction**

554 Biomass dynamics reflects the potential of vegetation to act as a carbon sink over the
555 long-term, as they integrate photosynthesis, autotrophic respiration and litter fall
556 fluxes (Thurner et al., 2014). Forest ecosystems cover more than 41 million km² of the
557 Earth's land surface and forests are thought to contain about half of the carbon in
558 terrestrial biomes (Prentice et al., 2001). Forests play an important role in the active
559 mitigation of atmospheric CO₂ through increased carbon stocks. The fixation of
560 atmospheric CO₂ into plant tissue through photosynthesis is one of the most effective
561 mechanisms for offsetting carbon emissions (Canadell and Raupach, 2008;
562 Gonzalez-Benecke et al., 2010).

563 Carbon sequestration by trees is the best way to store a large amount of terrestrial
564 carbon over long durations (Jung et al., 2013). Estimation of carbon stocks at scales
565 ranging from local to global is crucial for accurately predicting future changes in
566 atmospheric carbon dioxide (Yu et al., 2014). However, substantial uncertainties
567 remain in current model estimates of terrestrial carbon and there is an increasing need
568 to quantify and reduce these uncertainties (Barman et al., 2014; Ahlstrom et al.,
569 2012).

570 Several studies have estimated the forest carbon stocks in China. Piao et al.
571 (2005), for example, used a satellite-based approach and estimated that: (1) the total
572 forest biomass of China averaged 5.79 Pg C during the period 1981-1999, with an
573 average biomass density of 4.531 kg C m⁻²; and (2) the total forest biomass C stock
574 increased from 5.62 Pg C in the early 1980s to 5.99 Pg C by the end of the 1990s,
575 giving a total increase of 0.37 Pg C and an annual sequestration rate of 0.019 Pg C yr⁻¹.
576 Zhang et al. (2007), on the other hand, analyzed seven forest inventories from 1973 to
577 2008 and suggested that the total biomass carbon stocks of all forest types increased

578 by 65% during this period, reaching 8.12 Pg C in 2008.

579 Wang et al. (2007) used the Integrated Terrestrial Ecosystem C-budget model and
580 estimated that China's forests were a source of 21.0 ± 7.8 Tg C yr⁻¹ due to human
581 activities during the period 1901-1949 and that this flux increased to 122.3 ± 25.3 Tg C
582 yr⁻¹ due to intensified human activities during the period 1950-1987. However, these
583 forests became large sinks of 176.7 ± 44.8 Tg C yr⁻¹ during the period 1988-2001
584 owing to large-scale plantation and forest regrowth in previously disturbed areas (see
585 the description of the Grain for Green Program below) as well as climatic warming,
586 atmospheric CO₂ fertilization, and N deposition.

587 Yang and Guan (2008) utilized the continuous Biomass Expansion Factor (BEF)
588 method with field measurements of forests plots in different age classes and forest
589 inventory data, and showed that the carbon density of the forests in the Pearl River
590 Delta increased by 14.3% from 19.08 to 21.81 kg C m⁻² during the period 1989-2003.
591 Similarly, Piao et al. (2009) reported that China's terrestrial ecosystems were a net
592 carbon sink of 0.19-0.26 Pg carbon per year and that they absorbed 28-37% of the
593 fossil carbon emissions during the 1980s and 1990s. However, their results also
594 showed that northeast China is a net source of CO₂ to the atmosphere due to the
595 over-harvesting and degradation of forests, while southern China accounts for more
596 than 65% of the carbon sink, which can be attributed to regional climate change,
597 large-scale plantation programs initiated in the 1980s, and shrub recovery (Piao et al.,
598 2009).

599 Guo et al. (2010) used three different approaches – the mean biomass density
600 (MBD) method, the mean ratio (MR) method, and the continuous BEF method (CBM)
601 – with forest inventory data to estimate China's forest biomass C stocks and their
602 changes from 1984 to 2003. The MBD, MR, and CBM estimated that forest biomass

603 C stocks increased from 5.7 to 7.7, 4.2 to 6.2, and 4.0 to 5.9 Pg C, respectively.

604 Deng et al. (2011) deployed a GIS approach and defined the vegetation carbon
605 sink as the carbon sequestration from the atmosphere ($1.63 \times \text{NPP}$), the vegetation
606 carbon stock as the carbon content that aboveground vegetation holds, and the soil
607 carbon stock as the carbon content that soil organic matter holds. These authors
608 estimated vegetation and soil carbon stocks to 1.58 and 1.41 Pg C, respectively, in the
609 forest ecosystems of China for the period 1981-2000.

610 Ni (2013) used available national-scale information to estimate that: (1) the mean
611 vegetation carbon in China was 36.98 Pg and mean soil carbon was 100.75 Pg C; and
612 (2) that the forest and grassland sectors supported mean carbon stocks of 5.49 and
613 1.41 Pg C, respectively.

614 The aforementioned studies show that the forest ecosystems of China store
615 steadily increasing stocks of carbon and that these forest stands have great potential to
616 absorb more biomass carbon in the future due to large fractions of young and
617 middle-aged forests and programs to promote the conservation of soil and biological
618 resources.

619 All these published results, which relied on either ground- or
620 satellite-observation-based estimation, resulted in pronounced differences in carbon
621 stock estimates. The objective of this study was to evaluate if fusing these data
622 sources could reduce the uncertainty associated with the final carbon stock estimates.

623

624 **2. Data and Materials**

625 The forest distribution data were created by combining the Vegetation Map of the
626 People's Republic of China (Editorial Committee of Vegetation Map of China, 2007)
627 with a vegetation map produced from the forest inventory conducted during the period

628 from 2004 to 2008 (State Forestry Administration of China, 2009). The former
629 provides a detailed classification of plant functional types and describes the
630 phenological and regional character of forests in China, but it is not so exact. The
631 latter shows the forest distribution in the period of the forest inventory, but its
632 classification provides less information about plant functional types. The combination
633 of the two kinds of maps retains the advantages of both.

634 The forest distribution data covers 161 plant biomes, including five classes of
635 deciduous needle-leaved trees, 57 classes of evergreen needle-leaved trees, 39 classes
636 of deciduous broad-leaved trees, 56 classes of evergreen broad-leaved trees and four
637 classes of mixed trees (Fig01).

638

639

Fig01

640

641 The national forestry inventory database (FID) for the period 2004-2008 includes
642 160,000 permanent sample plots and 90,000 temporary sample plots scattered across
643 China. The biomass density of each forest type in each province was calculated from
644 timber volume, using a BEF (Fang et al., 2007). The biomass carbon density (BCD)
645 of each forest type in each province was calculated next by multiplying the biomass
646 density by a carbon factor (CF) (Li and Lei, 2010). And finally, the biomass carbon
647 stock (BCS) of each forest type in each province was calculated by multiplying the
648 BCD by the area of that forest type. The total BCS in China is a sum of the BCS of all
649 of the forest types in the 31 provinces of China, excluding Taiwan, Hong Kong and
650 Macao.

651 The following formulations were used to calculate the forest BCS in China:

$$652 \quad TCS = \sum_{i=1}^M \sum_{j=1}^N (A_{i,j} \cdot BCD_{i,j}) \cdot 10^{-12} \quad (1)$$

653 $BCD_{i,j} = W_{i,j} \cdot CF_i$ (2)

654 $W_{i,j} = BEF_i \cdot V_{i,j}$ (3)

655 $BEF_{i,j} = a_i + \frac{b_i}{V_{i,j}}$ (4)

656 where TCS is the total forest BCSs of China (Pg); $BCD_{i,j}$ is the area weighted
 657 biomass carbon density of the i th forest type in the j th province (kg/m^2); $A_{i,j}$ is the
 658 area of the i th forest type in the j th province (m^2); M and N refer to the numbers of
 659 forest types and provinces in China, respectively; $W_{i,j}$ is the area weighted mean
 660 forest biomass of the i th forest type in the j th province (kg / m^2); CF_i is the CF of the
 661 i th forest type; $V_{i,j}$ is the area weighted mean timber volume of the i th forest type in
 662 the j th province (m^3 / m^2); BEF_i is the BEF of the i th forest type (kg / m^3); and a_i
 663 (kg / m^3) and b_i (kg / m^2) are constants of the i th forest type to be simulated. The mean
 664 CF_i of all coniferous forest types was used for coniferous mixed forest. The mean
 665 CF_i of all broad-leaved forest types was used for broad-leaved mixed forest. The
 666 mean CF_i of all broad-leaved and coniferous forest types was used for broad-leaved
 667 and coniferous mixed forest.

668 The land mass of China was next divided into nine regions (Fig02) with similar
 669 temperature, precipitation and soil regimes to make it easier to analyze changes in
 670 forest carbon storage from one place to another (Zhou et al., 1981). The nine regions
 671 are referred to as R_k where $k = 1$ to 9 and we use periods 1, 2, 3, 4 and 5 to
 672 represent the periods 1984-1988, 1989-1993, 1994-1998, 1999-2003 and 2004-2008,
 673 respectively.

674

675
676
677

678 **3. Methods**

679 **3.1 Satellite-observation-based approach (SOA)**

680 The SOA used the normalized differential vegetation index (NDVI) at a temporal
681 resolution of one month and at a spatial resolution of 1 km x 1 km from the Earth
682 Observation System's moderate-resolution imaging spectroradiometer (EOS MODIS)
683 (Piao et al., 2009). The BCD from the FID data was matched with the NDVI data
684 using the forest map of China reproduced in Fig01.

685 The BCD mirrored the latitude, longitude and maximum value of the
686 monthly-averaged NDVI values during the Seventh National Forest Inventory
687 conducted from 2004 to 2008:

$$688 \quad BCD_j = 93.351 \ln(NDVI_j) - 2.96 Lat_j - 21.388 Lon_j + 0.047 Lat_j^2 + 0.091 Lon_j^2 + 1339.03 \quad (5)$$

689 where $NDVI_j$ is the mean of the maximum values of the monthly-averaged NDVI
690 values during the period 2004-2008 in the j th province and Lat_j and Lon_j refer to
691 the latitude and longitude of the center of the j th province, respectively. The
692 coefficient of correlation ($R=0.91$) and significance ($P<0.001$) show how latitude,
693 longitude, and NDVI explained 83% of the variability in BCD.

694

695 **3.2 High accuracy surface modeling (HASM)**

696 HASM was developed for efficiently fusing satellite- with ground-observations to
697 find solutions for error problems which have long troubled earth surface modeling
698 (Yue, 2011). HASM has been successfully used to construct digital elevation models

699 (Yue et al. 2007, 2010a, 2010b; Yue and Wang, 2010; Chen and Yue 2010; Chen et al.
700 2013a, b), model surface soil properties (Shi et al. 2011) and soil pollution (Shi et al.
701 2009), fill voids in the Shuttle Radar Topography Mission (SRTM) dataset (Yue et al.
702 2012), simulate climate change (Yue et al. 2013a, b; Zhao and Yue 2014a, b), fill
703 voids in remotely sensed XCO₂ surfaces (Yue et al. 2015a), and to analyze ecosystem
704 responses to climatic change (Yue et al. 2015b). In all of these applications, HASM
705 produced more accurate results than the classical methods (Yue et al., 2015c).

706

707 **3.3 Estimation of carbon stocks**

708 Forest carbon stocks and carbon densities were estimated by methods of spatial
709 interpolation, SOA and data fusion. The spatial interpolation provided an effective
710 approach to construct a continuous surface from the FID by means of Kriging; it took
711 advantage of limited observation data to estimate the most plausible spatial
712 distribution by filling in missing data. The data fusion approach integrated the forest
713 inventory and satellite data into a consistent, accurate and useful representation using
714 HASM (HASM-S) (see supplement 1 in details); the aim of the data fusion was to
715 improve the quality of the information so that it was more accurate than would be
716 possible if the data sources had been used individually.

717

718 **3.4 Validation**

719 The uncertainties of the carbon stock estimates reported in earlier studies relied on
720 several different concepts and metrics. The same formula for absolute and relative
721 error should be used to evaluate all estimates of carbon stocks so that the estimation
722 results are comparable. We calculated the mean absolute errors (MAE) and mean
723 relative errors (MRE), respectively, as:

724
$$MAE = \frac{1}{n} \sum_i^n |o_i - s_i| \quad (6)$$

725
$$MRE = \frac{MAE}{\frac{1}{n} \sum_i^n |o_i|} \quad (7)$$

726 where o_i represents the forest carbon stocks at the i th control point; s_i represents the
 727 simulated value at the i th control point; and n_i is the total number of control points
 728 used for validation.

729 Cross-validation is used to estimate how accurately a model performs, which is
 730 analyzed by removing certain data points in turn and summing the absolute value of
 731 the discrepancy of each removed data point from the simulated one at the same
 732 location (Hulme et al., 1995). It was comprised of four steps: (1) 5 % of the sample
 733 plots from the national forest inventory were removed for validation; (2) the spatial
 734 distribution of average forest BCSs in China during the period 2004-2008 were
 735 simulated at a spatial resolution of 5 km × 5 km using the remaining 95% of the
 736 sample plots from the national forest inventory by means of the different methods; (3)
 737 the MAEs and MREs were calculated using the 5% validation set; and (4) the 5%
 738 validation set was returned to the pool for the next iteration, and another 5%
 739 validation set was removed. This final process was repeated until all the sample plots
 740 were used for validation at least one time and the simulation error statistics could be
 741 calculated for each sample plot.

742

743 **4 Results**

744 The three maps of mean annual carbon stocks during the period 2004-2008
 745 reproduced with each of the aforementioned methods shows how the Kriging, SOA
 746 and HASM-S methods were able to generate the same overall patterns based on the

747 underlying forest cover, and how the estimates varied using each of these methods
748 over large parts of the China (Fig03). This variability raises questions related to the
749 reliability of the estimates produced with the three aforementioned approaches.

750

751

Fig03

752

753 The cross-validation results indicated that Kriging and SOA had larger errors,
754 with MREs of 50.12 and 48.77%, respectively. Kriging over-estimated the carbon
755 stocks, while SOA under-estimated the carbon stocks (Table 1). Accuracy was
756 considerably improved when the forest inventory and satellite data were fused by
757 using HASM-S. The MRE of HASM-S was 22.71%.

758

Table 1

760

761 The BCSs of all forest types estimated with HASM-S (the best approach) was
762 7.08 Pg in China during the period 2004-2008. The BCSs of coniferous, broadleaf and
763 mixed forests were 2.74, 3.95 and 0.39 Pg, respectively (Table 1). The mean carbon
764 densities (MBCDs) of the coniferous, broadleaf and mixed forests were 4.35, 4.74 and
765 4.20 kg/m², respectively.

766 The HASM-S estimates showed that 89.9% of the MBCSs were found in the
767 regions R5, R3, R6, R9 and R7 during the period P5, accounting for 28.61, 28.41,
768 14.48, 12.52 and 5.89% of the BCSs, respectively. The three largest BCDs occurred in
769 R5 (Tibet plateau; 10.53 kg/m²), R2 (arid area; 6.33 kg/m²) and R3 (northeastern
770 China; 4.44 kg/m²) (Table 2 and Fig03c). The two smallest BCDs were predicted in
771 the R8 (2.14 kg/m²) and R9 (2.60 kg/m²) regions.

772

773 **Table 2**

774

775 The HASM-S estimates can be parsed by forest type as well (Table 3). Hence, the
776 BCDs of evergreen broad-leaved and evergreen coniferous forests were 6.23 and 4.47
777 kg/m^2 , respectively, while the BCDs for deciduous broad-leaved and deciduous
778 coniferous forests were 3.93 and 3.77 kg/m^2 , respectively in P5. The BCD of
779 evergreen forests was 50% larger than that of deciduous forests, and the BCDs for
780 broad-leaved forests were greater than those for both coniferous and deciduous forests.
781 Turning next to the BCSs, the evergreen coniferous forests contributed the largest
782 proportion, accounting for 33.05%, followed by deciduous broad-leaved forests
783 (29.8%), and evergreen broad-leaved forests (25.99%). The deciduous coniferous and
784 the broad-leaved and coniferous mixed forests accounted for the two smallest
785 proportions of the total BCS, 5.65 and 5.51%, respectively.

786

787 **Table 3**

788

789 The HASM-S estimates also indicate that BCSs rose from 4.84 Pg in period 1 to
790 7.08 Pg in P5 due to the increase of BCD and the expansion of forest area (Table 4).
791 The BCD rose from 4.00 kg/m^2 in P1 to 4.55 kg/m^2 in P5 and the forest area grew
792 from 1.21 million km^2 in P1 to 1.56 million km^2 in P5. The increasing trends of the
793 BCS, BCD and forest area (FA) are captured by the following regression equations:

794 $BCS(t) = 0.531t + 4.297$ $R = 0.976$ (8)

795 $BCD(t) = 0.125t + 3.958$ $R = 0.943$ (9)

796 $FA(t) = 0.083t + 1.1045$ $R = 0.96$ (10)

797 where t corresponds to periods 1, 2, 3, 4 and 5; $BCS(t)$, $BCD(t)$ and $FA(t)$ are
798 BCS, BCD and FA, respectively in the period t ; and R represents the correlation

799 coefficient for the corresponding regression equation.

800

801 **Table 4**

802

803 Although BCS rose in all nine regions from period 1 to period 5, the spatial
804 variability over China more or less mirrors the variability in the distribution of forests
805 (Fig04, Fig05, Table 4). For regions R1 and R8, for example, both BCS and BCD
806 have continuously increased from period 1 to period 5. R8 has the smallest BCS,
807 which only accounted for 0.83% of the BCS of the whole of China, and the smallest
808 BCD of 2.14 kg/m^2 in P5 as well as the lowest BCS accumulation rate of $1.3 \text{ Tg}\cdot\text{yr}^{-1}$.
809 In R1, BCS accounted for 3.94% of the total BCS of China for the period of P5 and
810 the BCS accumulation rate has averaged $6.2 \text{ Tg}\cdot\text{yr}^{-1}$ from P1 to P5.

811

812 **Fig04**

813

814 **Fig05**

815

816 The region R5 had the largest BCS, accounting for 28.61% of the total BCS of
817 China in P5, along with the largest BCD of 10.53 kg/m^2 and the fastest BCS
818 accumulation rate of $52 \text{ Tg}\cdot\text{yr}^{-1}$; the BCS has shown a monotonically increasing trend
819 since P1. The second largest BCS occurred in R3 (Northeastern China). The BCS in
820 R3 accounted for 28.41% of the total BCS of China. However, the BCD in R3 has
821 declined since P3 following increases from P1 to P2 and from P2 to P3. The mean
822 BCS accumulation rate in R3 was 21.3 Tg/yr .

823 In the regions R4 (Loess Plateau), R6 and R9, both BCS and BCD have increased
824 since P3. The BCSs in R4, R6 and R9 accounted for 2.68, 14.48 and 12.26% of the

825 BCS in the whole of China in P5, respectively. The average BCS accumulation rates
 826 were 2.8, 10.4 and 12.7 Tg·yr⁻¹, respectively in R4, R6, and R9. In R2 (an arid area),
 827 the BCS accounted for 2.80% of the total for China in the period P5. The BCS and
 828 BCD increased from P4 to P5, but the mean accumulation rate of BCS was only 2.3
 829 Tg·yr⁻¹. The BCS accounted for 5.89% of the total for China in R7. The BCS and
 830 BCD both increased from P4 to P5 but like in R2, the mean BCS accumulation rate
 831 was relatively low at just 2.9 Pg·yr⁻¹.

832 In terms of forest types, evergreen broad-leaved forests had the fastest BCS
 833 accumulation rate and the largest BCD, while evergreen coniferous forests contributed
 834 the largest BCS. The BCSs of broad-leaved forests increased during all five periods.
 835 The BCS of evergreen broad-leaved forests increased from 0.63 Pg in period 1 to 1.84
 836 Pg in period 5, and the BCSs for deciduous broad-leaved forests rose from 1.38 Pg in
 837 period 1 to 2.11 Pg in period 5. These trends can be modeled with the following
 838 regression equations:

$$839 \quad BCS_1(t) = 0.312t + 0.286, \quad R = 0.998 \quad (11)$$

$$840 \quad BCS_2(t) = 0.199t + 1.115, \quad R = 0.981 \quad (12)$$

841 where t corresponds to period t , $t = 1, 2, 3, 4$ and 5 ; $BCS_1(t)$ and $BCS_2(t)$ are
 842 respectively the BCSs of evergreen broad-leaved forests and deciduous broad-leaved
 843 forests in the period t and R represents the correlation coefficient of the
 844 corresponding regression equation.

845 The BCSs of deciduous coniferous forests fluctuated from period to period.
 846 Evergreen coniferous forests and broad-leaved and coniferous mixed forests exhibited
 847 an increasing trend of BCS in general but declined in period 3. Their trends were
 848 modeled with the following regression equations:

$$849 \quad BCS_3(t) = 0.207t + 1.391, \quad R = 0.932 \quad (13)$$

850 $BCS_4(t) = 0.076t - 0.068$, $R = 0.867$ (14)

851 where t corresponds to periods 1, 2, 3, 4 and 5; $BCS_3(t)$ represents the BCSs of
852 evergreen coniferous forests in the period t ; $BCS_4(t)$ refers to the broad-leaved and
853 coniferous mixed forests; and R represents the correlation coefficient of the
854 corresponding regression equation.

855 The equations (8), (9) and (10) indicate that increasing rates of BCS, BCD and
856 FA were 0.531 Pg, 0.125 kg/ m² and 0.083 million km², respectively, over a five-year
857 period on average. According to equations (11) and (12), the BCS of evergreen
858 broad-leaved forests had a growth rate of 0.312 Pg over a five-year period, which was
859 0.113 Pg higher than that for deciduous broad-leaved forests because of the different
860 increasing rates of BCD; the BCD of evergreen broad-leaved forests increased by 1.87
861 kg/m², while the BCD of deciduous broad-leaved forests increased by 0.18 kg/m²
862 from period 1 to period 5. The equations (13) and (14) show that carbon stocks of
863 evergreen coniferous forests grew much faster than those for broad-leaved and
864 coniferous mixed forests. The former grew by 0.207 Pg but the latter by only 0.076 Pg
865 in a five-year period on average because the area of evergreen coniferous forests was
866 five times larger (0.50×10^6 km² compared to 0.09×10^6 km² for broad-leaved and
867 coniferous mixed forests) and offset the lower BCD growth rate of the former (0.132
868 kg/m²) compared to 0.56 kg/m² for broad-leaved and coniferous mixed forests per
869 five-year period.

870 The results from Kriging and HASM-S exhibit a similar spatial pattern on the
871 national level, especially in southern Tibet, the Xiao Hinggan Moutains, the Changbai
872 Mountains, and south China. Some differences occur in Taiwan and Xinjiang as well
873 as the Qinling Mountains. Compared to HASM-S, Kriging is strongly influenced by
874 sample-plot density. The spatial heterogeneity of the results from SOA is not so

875 obvious because NDVI, a critical variable of SOA, is not so sensitive to a change of
876 carbon stocks, especially in northeast China and near the lower reaches of Yangtze
877 River.

878 The scatter diagrams of simulated BCD against observed BCD (Fig06) indicate
879 that the BCD surface created by Kriging exhibits a higher correlation with observed
880 BCD, $R^2=0.826$. But the Kriging interpolation generated large errors in the
881 Xizang/Tibet and Xinjing regions, which have the highest BCD. The BCD was
882 overestimated in Xizang and underestimated in Xinjiang. The BCD surface created by
883 SOA has the lowest coefficient of determination, $R^2= 0.627$, with the observed one.
884 The SOA results show that BCDs in higher and lower latitudes are larger than those in
885 middle latitudes, but for Xinjiang and Xizang. The BCD was overestimated in
886 Xinjiang but underestimated in Xizang. The surface of BCDs generated by HASM-S
887 has the best correlation with the observed one, $R^2=0.943$ and it generated the smallest
888 errors in the regions of Xizang and Xinjiang, compared with the other methods.

889

890 Fig06

891

892 **5 Discussion and Conclusions**

893 HASM-S overcame the shortcomings of both the ground-based national forest
894 inventory and the satellite remote-sensing observations by fusing information about
895 the details of the carbon stocks observed on the Earth's surface and the variability of
896 the carbon surface observed from space. The cross-validation demonstrated that
897 HASM-S was 26.1% more accurate than the satellite-based approach and 28.4% more
898 accurate than spatial interpolation of the sample plots. These findings suggest that
899 China's forest biomass carbon stocks are more likely to be closer to our estimates than

900 those generated by past efforts to estimate these same carbon stocks and their change
901 over time.

902 Taken as a whole, the HASM-S results show that the forest carbon stocks of
903 China have increased by 2.24 Pg during the period 1984-2008 to a new high of 7.08
904 Pg C in 2008. These numbers fall in the middle of the previously published estimates.
905 All of the estimates show forest biomass carbon stocks in China increasing from 1973
906 to 2008, notwithstanding the various methods used and the varying levels of
907 uncertainty embedded in these different methods and the data sources used.

908 The results from HASM-S are compare favorably well with those of other studies.
909 For instance, the annual growth of total BCS from period 1 (circa 1986) to period 5
910 (circa 2006) in China was 0.112 PgCyr^{-1} . This estimate was higher than that of Zhang
911 et al. (2013), which was 0.103 PgCyr^{-1} . However, our estimate of 0.148 PgCyr^{-1} from
912 period 3 (circa 1996) to period 5 (circa 2006) was lower than the 0.174 PgCyr^{-1}
913 estimated by Zhang et al. (2013). From period 4 (circa 2001) to period 5 (circa 2006),
914 the 0.14 PgCyr^{-1} estimated by HASM-S was twice that estimated by Liu et al. (2015).

915 In recent years, there are several different vegetation biomass maps for
916 pan-tropical area (e.g. Avitabile *et al.*, 2016; Baccini *et al.*, 2012; Saatchi *et al.*, 2011).
917 They were based on combination of data from ground observations and satellite
918 remote sensing. The spatial distribution pattern of the forest biomass carbon at low
919 latitudes of China area simulated by HASM-S was consistent with the biomass carbon
920 maps for pan-tropical area, i.e. south of Tibet plateau had the highest biomass carbon
921 density, followed by southeast Tibet plateau, west of YunNan-GuiZhou plateau, the
922 area of QinLing mountains and DaBa mountains; Southeastern China has the lowest
923 forest biomass density except the area of Wuyi mountains. However, the biomass
924 carbon densities from HASM-S were lower than the one from Baccini et al. (2012),

925 especially in southeastern China.

926 The Grain for Green program, which was launched in 1999 and aims to restore
927 the country's forests and grasslands to prevent soil erosion, has emerged as one of the
928 key drivers of carbon sequestration in China. The increase in forest growth rate under
929 climate change may also contribute to sequestering more carbon, but has relatively
930 less impact than the restoration of forest lands or establishment of new forests (Gorte,
931 2009). This program targets land with slopes $> 25^\circ$ (Xu et al., 2006; Yue et al., 2010c)
932 and has been implemented in four phases: (1) a pilot phase (1999-2001); (2) an initial
933 construction phase (2002-2010); (3) a consolidation phase (2011-2013); and (4) a
934 second construction phase to be built around a new round of Grain for Green program
935 expenditures (2014-2020).

936 The pilot program launched in 1999 focused on three provinces: Gansu, Shaanxi
937 and Sichuan. Approximately 381,000 ha of farmland was converted into forestland
938 and 66,000 ha of bare land was reforested. In 2000, the program was expanded to 17
939 provinces, and the converted farmland and reforested bare land totals grew to 410,000
940 and 449,000 ha, respectively. By 2001, 20 provinces were involved in the program
941 and 420,000 and 563,000 ha of farm and bare land had been reforested, respectively
942 (Table 5). The national Grain for Green program was launched in China in 2002 and
943 by the end of 2010, 14.667 million ha of farmland had been converted to forest or
944 grassland and 17.333 million ha of bare land had been reforested. During the
945 consolidation phase from 2011 to 2013, scientific monitoring and management of the
946 converted and reforested lands was strengthened to help sustain the aforementioned
947 achievements of the Grain for Green program over the long-term.

948

949 **Table 5**

950

951 To grow and consolidate these gains, the potential for farmland conversion at the
952 county level during the period 2014-2020 was estimated in 2014 by counting up
953 farmers' voluntary applications to determine how large an area could be converted to
954 forest or grassland. By 2020, 2.827 million ha of farmland could be converted, which
955 includes 1.449 million ha of farmland with slopes $>25^\circ$, 1.133 million ha of cultivated
956 land threatened by desertification, and 247,000 ha of farmland with slopes between 15
957 and 25° around the Danjiangkou and Three Gorges reservoirs.

958 The results from this latest phase of the Grain for Green program are encouraging.
959 Participating farmers can choose whether farmland is to be converted to forest or
960 grassland, and which species will be planted, and they will receive a 22,500 RMB
961 subsidy for every hectare of farmland converted to forest or grassland. In 2014,
962 322,000 ha were converted to forest and 11,000 ha were converted to grassland, and
963 in 2015 another 667,000 ha of farmland will be converted to either forest or grassland.

964 The BCS growth was improved by already existing forests and newly planted
965 forests. The former accounted for about 55% while the latter about 40%. The BCS in
966 existing forests had a growth rate of about 0.55 kg/m^2 per five-year period and the
967 BCS in newly planted forests grew at 1.8 kg/m^2 per five-year period.

968 Methodologically, the fusion of forest inventory data with satellite observations
969 achieved with HASM-S provided much more accurate estimates of forest biomass
970 carbon stocks and their changes. This kind of method can increase our understanding
971 of the role of forests in the carbon cycle, and help to support greenhouse gas
972 inventories and terrestrial carbon accounting projects (Muukkonen and Heiskanen,
973 2007).

974 However, HASM-S still has some limitations: 1) it can only simulate a surface of
975 carbon stocks at a specific time or the average condition for a period when there are

976 ground observations; in other words, it is difficult to use this approach to estimate
977 changes at higher temporal resolutions; and 2) it cannot generate and capture the
978 likely impacts of future interventions and scenarios. For finding solutions to these
979 limitations, we aim to develop a method for data assimilation which combines HASM
980 and the Dynamic Global Vegetation Model developed jointly by Lund University,
981 Potsdam Institute for Climate Impact Research and the Max Planck Institute for
982 Biogeochemistry Jena (LPJ-DGVM) (Sitch et al., 2003), so that surfaces of carbon
983 stocks could be simulated with less uncertainty in time series ranging from the past to
984 the present and for user-specified periods in the future. Future research should aim at
985 improving uncertainty estimates by deriving confidence intervals in the estimated
986 carbon stocks by applying the basic principles of sampling theory and/or using models
987 that contains the code for uncertainty analysis, such as the Monte Carlo approach.
988 Uncertainty estimates can allow decision makers to better appreciate the amplitude of
989 the errors in carbon stock estimates. For researchers, uncertainty estimates may
990 contribute to improving methodologies to estimate carbon stocks.

991

992 *Acknowledgments.* This work was supported by the National Natural Science
993 Foundation of China (91325204), by the National High-tech R&D Program of the
994 Ministry of Science and Technology of the People's Republic of China
995 (2013AA122003), and by the National Basic Research Priorities Program
996 (2010CB950904) of the Ministry of Science and Technology of the People's Republic
997 of China.

998

999 **References**

1000 Ahlstrom, A., Schurgers, G., Arneeth, A. and Smith, B.: Robustness and uncertainty

1001 in terrestrial ecosystem carbon response to CMIP5 climate change projections,
1002 Environmental Research Letters, 7, 044008, 2012.

1003 Avitabile, V., and other 33 coauthors: An integrated pan-tropical biomass maps using
1004 multiple reference datasets. *Global Change Biology*, 22, 1406–1420, 2016.

1005 Baccini, A., and other 11 coauthors: Estimated carbon dioxide emissions from tropical
1006 deforestation improved by carbon-density maps. *Nature Climate Change*, 2,
1007 182–185, 2012.

1008 Barman, R., Jain, A.K. and Liang, M.L.: Climate-driven uncertainties in modeling
1009 terrestrial gross primary production: A site level to global-scale analysis, *Global*
1010 *Change Biology*, 20, 1394-1411, 2014.

1011 Canadell, J.G. and Raupach, M.R.: Managing forests for climate change mitigation,
1012 *Science*, 320, 1456-457, 2008.

1013 Chen, C.F., Li, Y.Y. and Yue, T.X.: Surface modeling of DEMs based on a sequential
1014 adjustment method, *International Journal of Geographical Information Science*,
1015 27, 1272-1291, 2013b.

1016 Chen, C.F., Yue, T.X., Dai, H.L. and Tian, M.Y.: The smoothness of HASM,
1017 *International Journal of Geographical Information Science* 27, 1651-1667, 2013a.

1018 Deng, S.H., Shi, Y.Q., Jin, Y. and Wang, L.H.: A GIS-based approach for quantifying
1019 and mapping carbon sink and stock values of forest ecosystem: A case study,
1020 *Energy Procedia*, 5, 1535-1545, 2011.

1021 Editorial Committee of Vegetation Map of China: *Vegetation Map of the People's*
1022 *Republic of China*. Geological Publishing House, Beijing, 2007 (in Chinese).

1023 Gonzalez-Benecke, C.A., Martin, T.A., Cropper Jr., W.P. and Bracho, R.: Forest
1024 management effects on in situ and ex situ slash pine forest carbon balance, *Forest*
1025 *Ecology and Management*, 260, 795-805, 2010.

1026 Forte, R.W.: Carbon sequestration in forests. Congressional Research Service Report
1027 for Congress 7-5700, 23p, 2009.

1028 Guo, Z.D., Fang, J.Y., Pan, Y.D. and Birdsey, R.: Inventory-based estimates of forest
1029 biomass carbon stocks in China: A comparison of three methods, *Forest Ecology
1030 and Management*, 259, 1225-1231, 2010.

1031 Hulme, M., Conway, D., Jones, P.D., Jiang, T., Barrow, E.M., Turney, C.: Construction
1032 of a 1961-1990 European climatology for climate change modelling and impact
1033 applications, *International Journal of Climatology* 15, 1333-1363, 1995.

1034 Jung, J., Kim, S., Hong, S., Kim, K., Kim, E., Im, J. and Heo, J.: Effects of national
1035 forest inventory plot location error on forest carbon stock estimation using
1036 k-nearest neighbor algorithm, *ISPRS Journal of Photogrammetry and Remote
1037 Sensing*, 81, 82-92, 2013.

1038 Li, H.K. and Lei, Y.C.: Estimation and Evaluation of Forest Biomass Carbon Storage
1039 in China, China Forestry Press (in Chinese), Beijing, 2010.

1040 Liu, Y.Y., van Dijk, A.I.J.M., de Jeu, R.A.M., Canadell, J.G., McCabe, M.F., Evans,
1041 J.P., Wang, G.J.: Recent reversal in loss of global terrestrial biomass. *Nature
1042 Climate Change*, DOI: 10.1038/NCLIMATE2581, 2015.

1043 Muukkonen, P. and Heiskanen, J.: Biomass estimation over a large area based on
1044 standwise forest inventory data and ASTER and MODIS satellite data: A
1045 possibility to verify carbon inventories, *Remote Sensing of Environment*, 107,
1046 617-624, 2007.

1047 Office of Converting Farmland to Forestry, State Forestry Administration of China: A
1048 new round of the overall concept of returning farmland to forest and grass,
1049 *Newsletter for Converting Farmland to Forestry*, 194, 1-2, 2014 (in Chinese).

1050 Office of Converting Farmland to Forestry, State Forestry Administration of China:
1051 New Year's Speech, Newsletter for Converting Farmland to Forestry, 198, 1-2,
1052 2016 (in Chinese).

1053 Piao, S.L., Fang, J.Y., Ciais, P., Peylin, P., Huang, Y., Sitch, S. and Wang, T.: The
1054 carbon balance of terrestrial ecosystems in China, *Nature*, 458, 1009-1014, 2009.

1055 Piao, S.L., Fang, J.Y., Zhu, B. and Tan, K.: Forest biomass carbon stocks in China
1056 over the past 2 decades: Estimation based on integrated inventory and satellite
1057 data, *Journal of Geophysical Research*, 110, G01006, 2005.

1058 Prentice, I.C., and other 36 coauthors: The carbon cycle and atmospheric carbon
1059 dioxide. In Houghton, J.T., Ding, Y., Griggs, D.J., Noguer, M., Van Der Linden,
1060 P.J., Dai, X., Maskell, K., Johnson, C.A. (Eds.) *Climate Change 2001: The
1061 Scientific Basis*. Cambridge, Cambridge University Press, 183-237, 2001.

1062 Saatchi, S.S., and other 14 coauthors: Benchmark map of forest carbon stocks in
1063 tropical regions across three continents. *Proceedings of the National Academy
1064 of Sciences*, 108, 9899–9904, 2011.

1065 Shi, W.J., Liu, J.Y., Song, Y.J., Du, Z.P., Chen, C.F. and Yue, T.X.: Surface modeling
1066 of soil pH, *Geoderma*, 150, 113-119, 2009.

1067 Sitch, S., Smith, B., Prentice, I.C., Arneth, A., Bondeau, A., Cramer, W., Kaplan, J.O.,
1068 Levis, S., Lucht, W., Sykes, M.T., Thonicke, K. and Venevsky, S. 2003.
1069 Evaluation of ecosystem dynamics, plant geography and terrestrial carbon cycling
1070 in the LPJ Dynamic Global Vegetation Model, *Global Change Biology* 9,
1071 161-185.

1072 State Forestry Administration of China: National Forest Report (2004-2008), China
1073 Forestry Publishing House, Beijing, 2009 (in Chinese).

1074 Thurner, M., Beer, C., Santoro, M., Carvalhais, N., Wutzler, T., Schepaschenko, D.,

1075 Shvidenko, A., Kompter, E., Ahrens, B., Levick, S.R. and Schmillius, C.: Carbon
1076 stock and density of northern boreal and temperate forests, *Global Ecology and*
1077 *Biogeography*, 23, 297-310, 2014.

1078 Wang, S., Chen, J.M., Ju, W.M., Feng, X., Chen, M., Chen, P. and Yu, G.: Carbon
1079 sinks and sources in China's forests during 1901-2001, *Journal of Environmental*
1080 *Management*, 85, 524-537, 2007.

1081 Xu, Z.G., Xu, J.T., Deng, X.Z., Huang, J.K., Uchida, E. and Rozelle, S.: Grain for Green
1082 versus grain: Conflict between food security and conservation set-aside in China,
1083 *World Development*, 34, 130-148, 2006.

1084 Yang, K. and Guan, D.S.: Changes in forest biomass carbon stock in the Pearl River
1085 Delta between 1989 and 2003, *Journal of Environmental Sciences*, 20, 1439-1444,
1086 2008.

1087 Yu, G.R., Chen, Z., Piao, S.L., Peng, C.H., Ciais, P., Wang, Q.F., Li, X.R. and Zhu,
1088 X.J.: High carbon dioxide uptake by subtropical forest ecosystems in the East
1089 Asian monsoon region, *Proceedings of the National Academy of the Sciences of*
1090 *the USA*, 111, 4910-4915, 2014.

1091 Yue, T.X., Liu, Y., Zhao, M.W., Du, Z.P., Zhao, N.: A fundamental theorem of
1092 Earth's surface modelling. *Environmental Earth Sciences*, 75(9), article 751
1093 (pages 1 -12), 2016.

1094 Yue, T.X., Du, Z.P., Lu, M., Fan, Z.M., Wang, C.L., Tian, Y.Z. and Xu, B.: Surface
1095 modelling of ecosystem responses to climatic change, *Ecological Modelling*, 306,
1096 16-23, 2015a.

1097 Yue, T.X., Zhao, M.W. and Zhang, X.Y.: A high-accuracy method for filling voids on
1098 remotely sensed XCO₂ surfaces and its verification, *Journal of Cleaner*
1099 *Production*, 103, 819-827, 2015b.

1100 Yue, T.X., Zhang, L.L., Zhao, N., Zhao, M.W., Chen, C.F., Du, Z.P., Song, D.J., Fan,
1101 Z.M., Shi, W.J., Wang, S.H., Yan, C.Q., Li, Q.Q., Sun, X.F., Yang, H., Wang,
1102 C.L., Wang, Y.F., Wilson, J.P., and Xu, B.: A review of recent developments in
1103 HASM, *Environmental Earth Sciences*, 74(8), 6541-6549, 2015c.

1104 Yue, T.X., Zhao, N., Yang, H., Song, Y.J., Du, Z.P., Fan, Z.M. and Song, D.J.: The
1105 multi-grid method of high accuracy surface modelling and its validation,
1106 *Transactions in GIS*, 17, 943-952, 2013a.

1107 Yue, T.X., Zhao, N., Ramsey, R.D., Wang, C.L., Fan, Z.M., Chen, C.F., Lu, Y.M. and
1108 Li, B.L.: Climate change trend in China, with improved accuracy, *Climate*
1109 *Change*, 120, 137-151, 2013b.

1110 Yue, T.X., Chen, C.F. and Li, B.L.: A high accuracy method for filling SRTM voids
1111 and its verification, *International Journal of Remote Sensing*, 33, 2815–2830,
1112 2012.

1113 Yue, T.X.: *Surface Modelling: High Accuracy and High Speed Methods*, CRC Press,
1114 Boca Raton, FL, 2011.

1115 Yue, T.X., Chen, C.F. and Li, B.L.: An adaptive method of high accuracy surface
1116 modeling and its application to simulating elevation surfaces, *Transactions in GIS*,
1117 14, 615-630, 2010a.

1118 Yue, T.X., Song, D.J., Du, Z.P. and Wang, W.: High-accuracy surface modelling and
1119 its application to DEM generation, *International Journal of Remote Sensing*, 31,
1120 2205-2226, 2010b.

1121 Yue, T.X. and Wang, S.H.: Adjustment computation of HASM: A high-accuracy and
1122 high-speed method, *International Journal of Geographical Information Science*,
1123 24, 1725–1743, 2010.

1124 Yue, T.X., Wang, Q., Lu, Y.M., Xin, X.P., Zhang, H.B. and Wu, S.X.: Change trends

1125 of food provisions in China, *Global and Planetary Change*, 72(3), 118-130,
1126 2010c.

1127 Yue, T.X., Du, Z.P., Song, D.J. and Gong, Y.: A new method of surface modeling and
1128 its application to DEM construction, *Geomorphology*, 91, 161-172, 2007.

1129 Zhang, C.H., Ju, W.M., Chen, J.M., Zan, M., Li, D.Q., Zhou, Y.L. and Wang, X.Q.:
1130 China's forest biomass carbon sink based on seven inventories from 1973 to 2008,
1131 *Climatic Change*, 118, 933-948, 2013.

1132 Zhao, N. and Yue, T.X.: A modification of HASM for interpolating precipitation in
1133 China, *Theoretical and Applied Climatology*, 116, 273-285, 2014a.

1134 Zhao, N. and Yue, T.X.: Sensitivity studies of a high accuracy surface modelling
1135 method, *Science China-Earth Science*, 57, 1-11, 2014b.

1136 Zhou, L.S., Sun, H., Shen, Y.Q., Deng, J.Z., Shi, Y.L.: *Comprehensive Agricultural*
1137 *Planning of China*, China Agricultural Press, Beijing (in Chinese), 1981.

1138

1139

1140

1141

1142

1143

1144

1145

1146

1147

1148

1149

1150

1151 **Table 1. Biomass carbon stocks and biomass carbon densities as well as their errors produced by different**
1152 **methods.**

Method	Calculated object	Coniferous forests	Mixed forests	Broadleaf forests	Total	MAE (kg m⁻²)	MRE (%)
SOA	BCS (Pg)	2.48	0.46	3.61	6.55	1.92	48.77
	BCD (kg m ⁻²)	3.94	4.93	4.34			
Kriging	BCS (Pg)	2.76	0.39	4.11	7.26	1.97	50.12
	BCD (kg m ⁻²)	4.38	4.24	4.94			
HASM-S	BCS (Pg)	2.74	0.39	3.95	7.08	0.89	22.71
	BCD (kg m ⁻²)	4.35	4.2	4.74			

1153

1154

1155

1156

1157

1158

1159

1160

1161

1162

1163

1164

1165

1166

1167

1168

1169

1170 **Table 2. BCS and BCD of the forests in the nine regions of China during the periods 2004-2008 and**
 1171 **1984-1988**

Regions	P5 (from 2004 to 2008)			P1 (from 1984 to 1988)		BCS accumulation rate (Tg·yr ⁻¹)
	BCD kg·m ⁻²	BCS (Pg)	Percentage (%)	BCD kg·m ⁻²	BCS (Pg)	
R1	3.710	0.28	3.94	2.666	0.16	6.2
R2	6.330	0.20	2.80	6.358	0.15	2.3
R3	4.445	2.01	28.41	4.493	1.59	21.3
R4	3.274	0.19	2.68	3.035	0.13	2.8
R5	10.525	2.03	28.61	6.718	0.99	52.0
R6	3.671	1.03	14.48	3.734	0.82	10.4
R7	3.693	0.42	5.89	3.643	0.36	2.9
R8	2.138	0.06	0.83	1.515	0.03	1.3
R9	2.598	0.87	12.26	2.358	0.62	12.7
Total		7.08	100		4.84	112

1172
 1173
 1174
 1175
 1176
 1177
 1178
 1179
 1180
 1181
 1182
 1183
 1184
 1185
 1186
 1187
 1188
 1189
 1190

1191 **Table 3. BCSs and BCDs for all forest types during the five periods estimated using HASM-S**

Period	Calculation object	Deciduous coniferous forests	Evergreen coniferous forests	Broad-leaved and coniferous mixed forests	Deciduous broad-leaved forests	Evergreen broad-leaved forests
P1	BCS (Pg)	0.41	1.50	0.06	1.38	0.63
	BCD (kg/m²)	4.35	3.81	3.08	3.75	4.35
P2	BCS (Pg)	0.39	1.80	0.09	1.44	0.87
	BCD (kg/m²)	4.28	4.13	3.75	3.77	5.65
P3	BCS (Pg)	0.44	2.23	0.07	1.66	1.20
	BCD (kg/m²)	4.20	4.09	3.03	3.87	6.35
P4	BCS (Pg)	0.47	2.19	0.19	1.97	1.57
	BCD (kg/m²)	4.37	4.40	5.18	3.89	7.49
P5	BCS (Pg)	0.40	2.34	0.39	2.11	1.84
	BCD (kg/m²)	3.77	4.47	4.20	3.93	6.22

1192

1193

1194

1195

1196

1197

1198

1199

1200

1201

1202

1203

1204

1205

1206

Table 4. Biomass carbon stocks and biomass carbon densities estimated by HASM-S

Regions	Calculation	Period	Period	Period	Period	Period
	object	1	2	3	4	5
R1	BCS (Pg)	0.16	0.17	0.17	0.2	0.28
	BCD (kg m ⁻²)	2.67	2.71	2.88	2.98	3.71
R2	BCS (Pg)	0.15	0.16	0.15	0.18	0.2
	BCD (kg m ⁻²)	6.36	6.27	6.25	6.23	6.33
R3	BCS (Pg)	1.59	1.64	1.64	1.77	2.01
	BCD (kg m ⁻²)	4.49	4.42	4.5	4.43	4.44
R4	BCS (Pg)	0.13	0.15	0.14	0.16	0.19
	BCD (kg m ⁻²)	3.04	3.23	3.13	3.15	3.27
R5	BCS (Pg)	0.99	1.57	1.64	1.94	2.03
	BCD (kg m ⁻²)	6.72	10.15	10.83	11.49	10.53
R6	BCS (Pg)	0.82	0.87	0.82	0.96	1.03
	BCD (kg m ⁻²)	3.73	3.78	3.66	3.88	3.67
R7	BCS (Pg)	0.36	0.39	0.37	0.4	0.42
	BCD (kg m ⁻²)	3.64	3.79	3.66	3.54	3.69
R8	BCS (Pg)	0.03	0.04	0.04	0.05	0.06
	BCD (kg m ⁻²)	1.52	1.64	1.89	1.89	2.14
R9	BCS (Pg)	0.62	0.56	0.62	0.73	0.87
	BCD (kg m ⁻²)	2.36	2.05	2.3	2.51	2.6
The whole of China	BCS (Pg)	4.84	5.55	5.6	6.38	7.08
	BCD (kg m ⁻²)	4	4.32	4.33	4.47	4.55
	Area (million km ²)	1.2101	1.2864	1.292	1.4279	1.5559

1208

1209

1210

1211

1212

1213

1214

1215

1216 **Table 5. Converted farmland and reforested bare land included in China's Grain for Green Program**
1217 **(millions hectares)** (Office of Converting Farmland to Forestry, State Forestry Administration of China,
1218 2014, 2016)

Year	Converted farmland	Afforestation on bare land	Total
1999	0.381	0.066	0.448
2000	0.405	0.468	0.872
2001	0.42	0.563	0.983
2002	2.647	3.082	5.729
2003	3.367	3.767	7.133
2004	0.667	3.333	4
2005	1.114	1.321	2.435
2006-2010	5.666	4.733	10.4
2014	0.333		0.333
2015	0.667		0.667
1999-2015	15.667	17.333	33
2016-2020	1.827		1.827

1219

1220

1221

1222

1223

1224

1225

1226

1227

1228

1229

1230

1231

1232

1233 **Table 6. List of Abbreviations**

Abbreviation	Explanation
BCD	Biomass Carbon Density
BCS	Biomass Carbon Stock
BEF	Biomass Expansion Factor (method)
CBM	Continuous BEF Method
CF	Carbon Factor
DGVM	Dynamic Global Vegetation Model
EOS	Earth Observation System
FA	Forest Area
FID	Forestry Inventory Database
HASM	High Accuracy Surface Modeling (method)
LPJ	Lund University, Potsdam Institute for Climate Impact Research and Max Planck Institute for Biogeochemistry, Jena
MAE	Mean Absolute Error
MBCD	Mean Biomass Carbon Density
MBD	Mean Biomass Density
MRE	Mean Relative Error
MODIS	Moderate-Resolution Imaging System
MR	Mean Ratio
NDVI	Normalized Difference Vegetation Index
NPP	Net Primary Productivity
SOA	Satellite-Observation-based Approach

1234

1235

1236

1237

1238

1239

1240

1241

1242

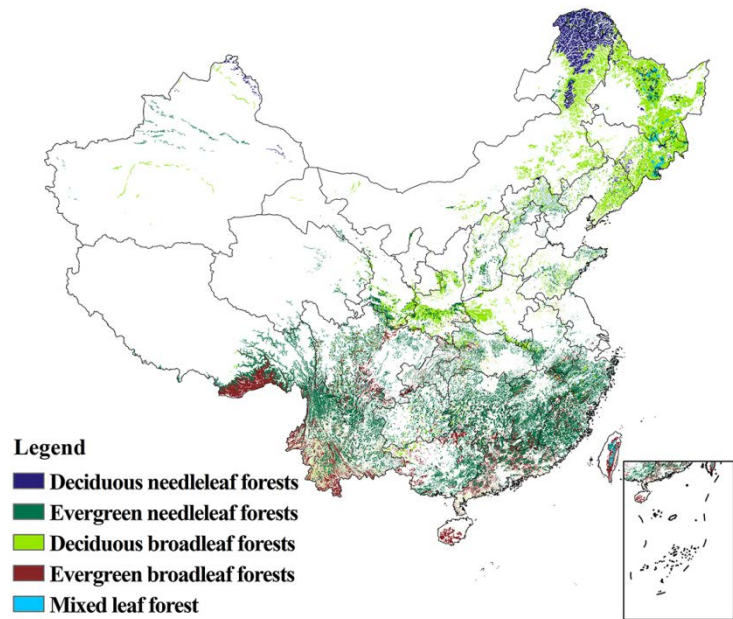
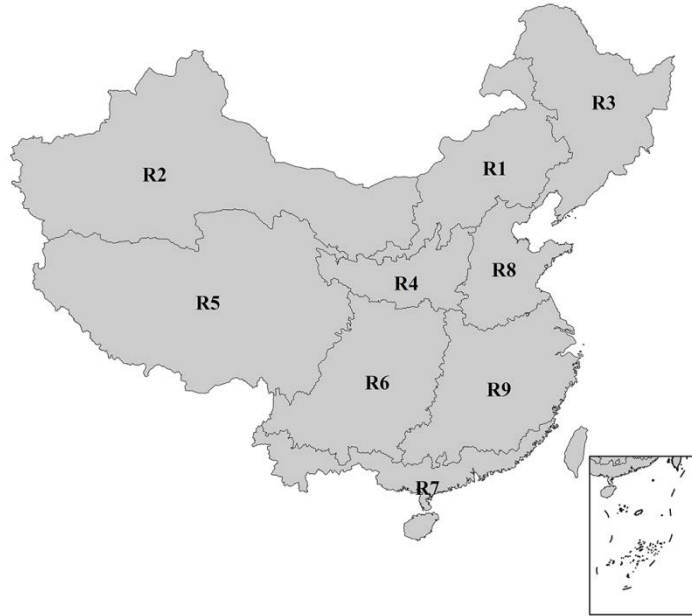


Fig01. The forest cover map of China

- 1243
- 1244
- 1245
- 1246
- 1247
- 1248
- 1249
- 1250
- 1251
- 1252
- 1253
- 1254
- 1255
- 1256
- 1257
- 1258
- 1259
- 1260
- 1261
- 1262
- 1263
- 1264



1265

1266

Fig02. Map showing the nine regions of China used for detailed analysis

1267

1268

1269

1270

1271

1272

1273

1274

1275

1276

1277

1278

1279

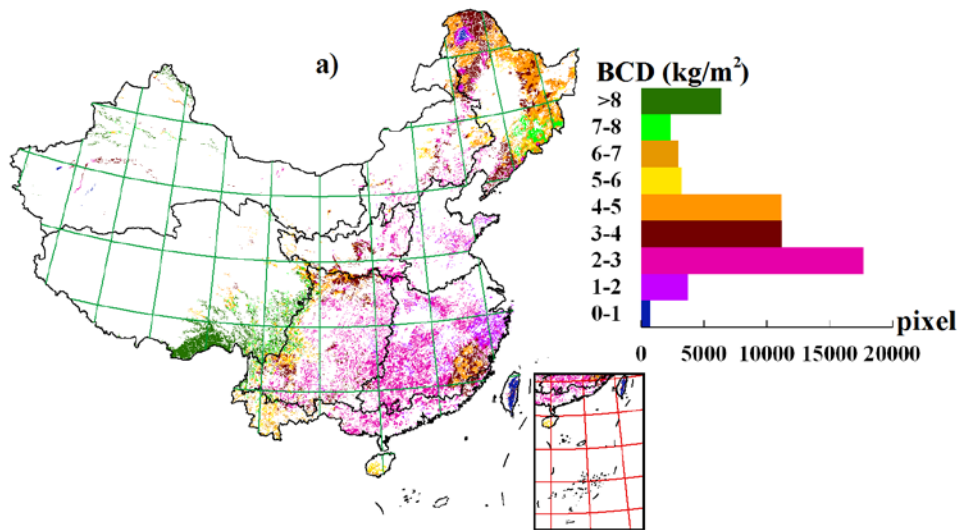
1280

1281

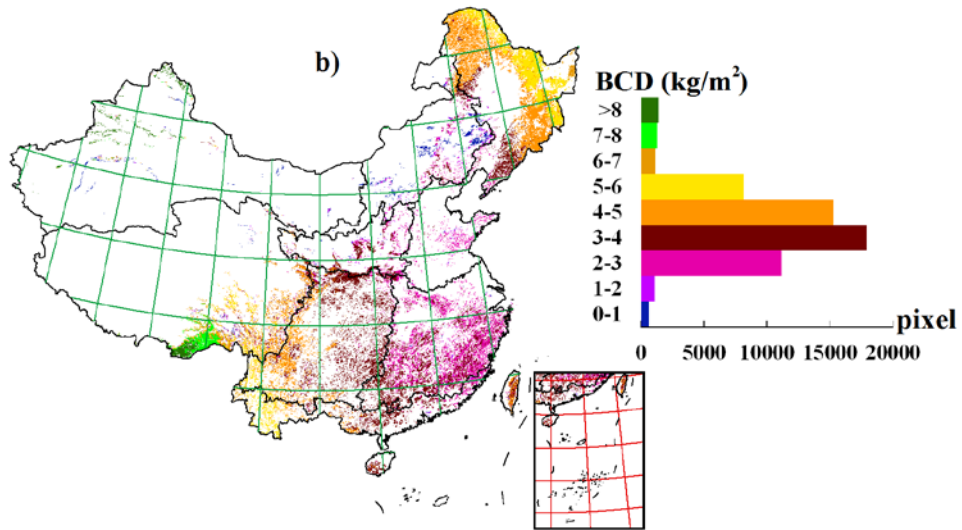
1282

1283

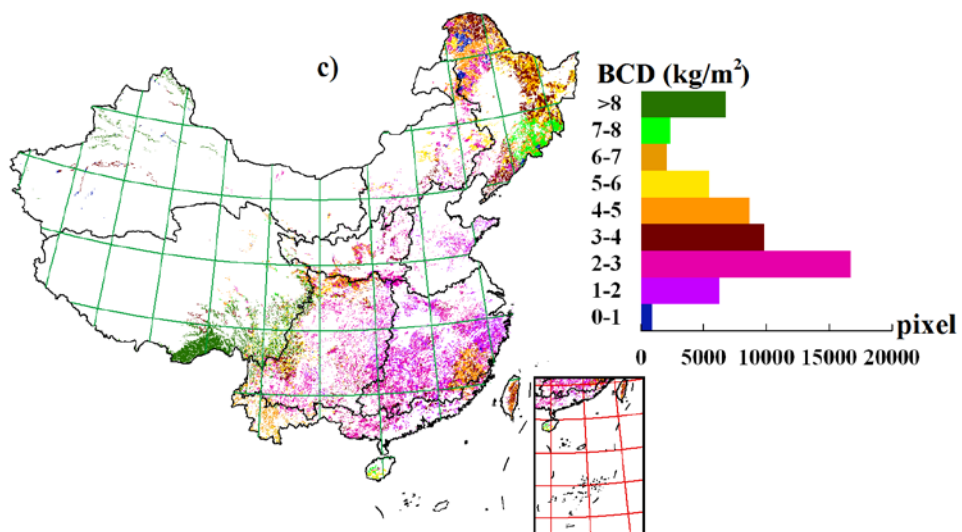
1284



1285



1286



1287

1288

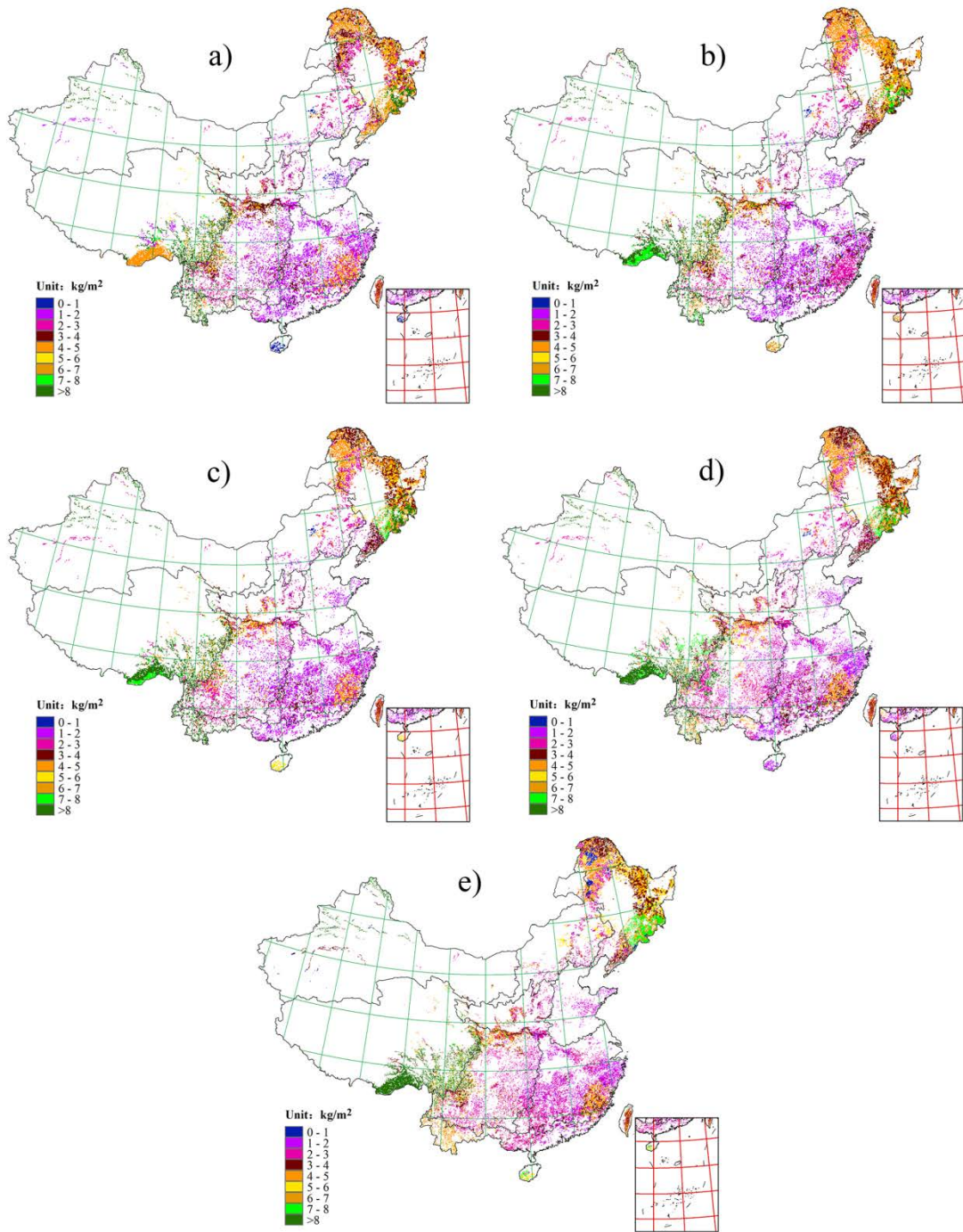
Fig03. The spatial distribution of forest biomass BCDs estimated during the period 2004-2008 in China

1289

using: (a) Kriging; (b) SOA; and (c) HASM-S

1290

1291



1292

1293 **Fig04. The spatial distribution of forest BCDs in China estimated during the five periods using HASM-S: (a)**

1294 **1984-1988 (P1); (b) 1989-1993 (P2); (c) 1994-1998 (P3); (d) 1999-2003 (P4); and (e) 2004-2008 (P5)**

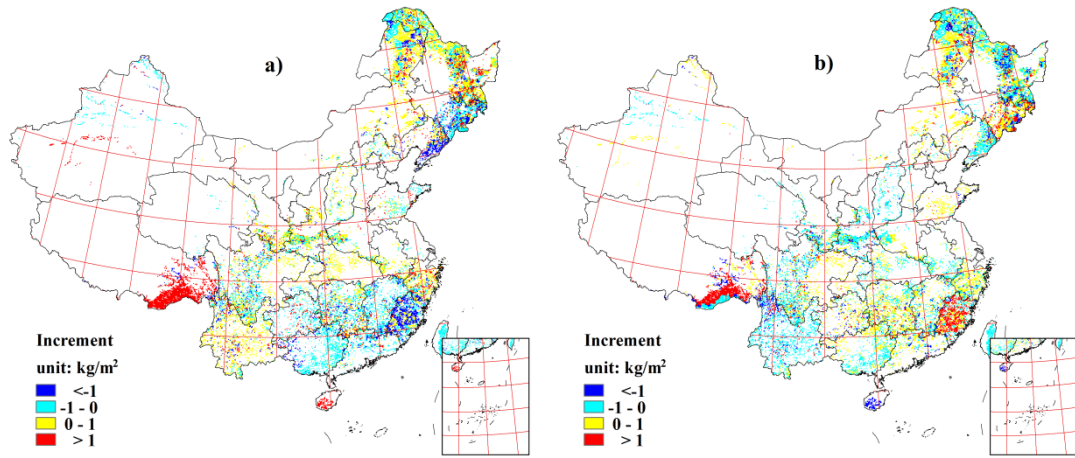
1295

1296

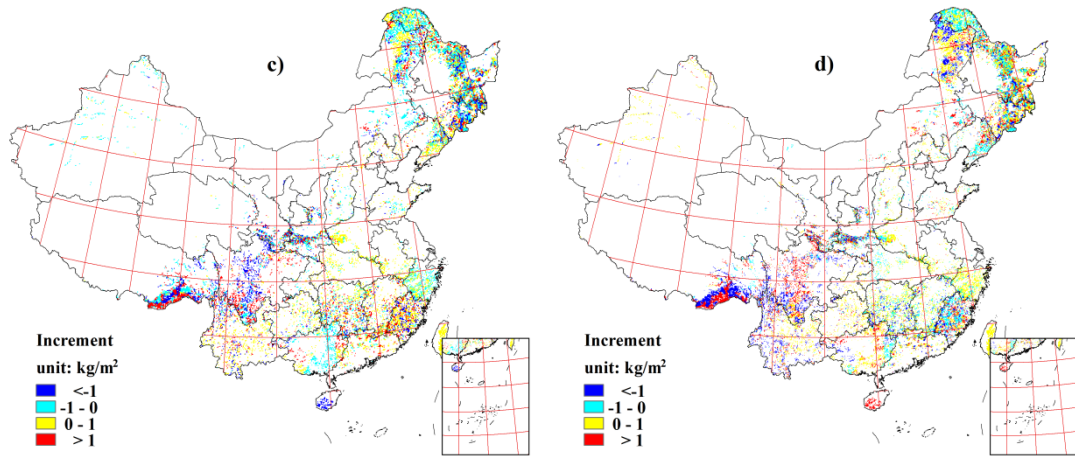
1297

1298

1299



1300



1301

1302 **Fig05. The increment maps of biomass carbon stocks from comparing two adjacent periods : a) BCS in**
1303 **Period 2 minus BCS in Period 1, b) BCS in Period 3 minus BCS in Period 2, c) BCS in Period 4 minus BCS in**
1304 **Period 3, and d) BCS in Period 5 minus BCS in Period 4**

1305

1306

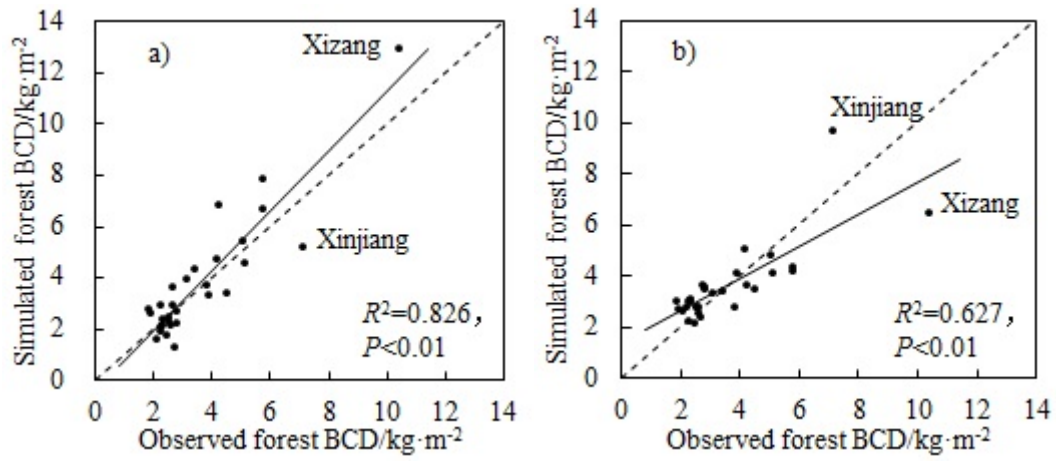
1307

1308

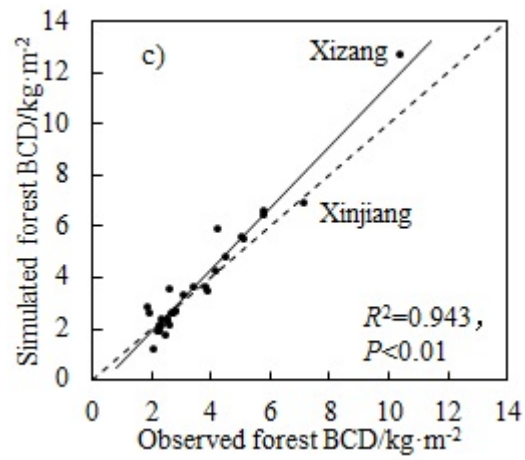
1309

1310

1311



1312



1313

1314 Fig06. The scatter diagrams of simulated BCD against observed BCD: a) Kriging, b) SOA, and c) HASM-S